Published in final edited form as:
Biomaterials. 2011 September ; 32(26): 6291–6301. doi:10.1016/j.biomaterials.2011.05.024.

Magnetic brain tumor targeting and biodistribution of long-circulating PEG-modified, cross-linked starch coated iron oxide nanoparticles

Adam J. Cole[1], **Allan E. David**[1,3], **Jianxin Wang**[1,4], **Craig J. Galbán**[2], and **Victor C. Yang**[1,5,*]

[1]Department of Pharmaceutical Sciences, College of Pharmacy, University of Michigan, Ann Arbor, Michigan 48109-1065, USA

[2]Department of Radiology, Center for Molecular Imaging, Medical School, University of Michigan, Ann Arbor, Michigan 48109-2200, USA

[3]Industrial Science & Technology Network Inc., York, PA 17404, USA

[4]Department of Pharmaceutics, School of Pharmacy, Fudan University, Shanghai 201203, China

[5]School of Pharmacy, Tianjin Medical University & Tianjin Key Laboratory for Modern Drug Delivery and High Efficiency, Tianjin 300070, China

Abstract

Magnetic iron oxide nanoparticles (MNPs) have been studied to circumvent the limitations of status-quo brain tumor therapy and can be targeted by applying an external magnetic field to lesions. To address the pharmacokinetic challenges of MNPs that can limit targeting efficiency, we recently reported a long-circulating polyethylene glycol modified, cross-linked starch MNP (PEG-MNP) suitable for magnetic targeting. Using a rat model, this work explores the biodistribution patterns of PEG-MNPs in organs of elimination (liver, spleen, lung, and kidney) and shows proof-of-concept that enhanced magnetic brain tumor targeting can be achieved due to improvements in the circulation lifetime of MNPs. Reductions in liver (~12 fold) and spleen (~2.5 fold) concentrations at 1 hr compared to parent starch MNPs (D) confirm plasma pharmacokinetics observed previously. While liver concentrations of PEG-MNPs remained considerably lower than those observed for D at 1 hr throughout their plasma clearance, spleen values continue to increase through and are markedly higher at 12 and 60 hr – a trend also observed with histology. Limited to no uptake of PEG-MNPs was visualized in lung or kidney throughout the 60 hr course evaluated. Enhanced, selective magnetic brain tumor targeting (t = 1 hr, 12 mg Fe/kg) of PEG-MNPs was confirmed in 9L glioma tumors, with upto 1.0% injected dose/g tissue accumulation achieved – a 15-fold improvement over targeted D (0.07% injected dose/g tissue). MRI and histological analyses visually confirmed enhanced PEG-MNP delivery to tumors and also suggest limited passive contribution to tissue retention of nanoparticles. Nonetheless, our results are exciting and justify both further development of PEG-MNP as a drug delivery platform and concurrent optimization of the magnetic brain tumor targeting strategy utilized.

*Correspondence and reprint request should be addressed to: Victor C. Yang, Ph.D., Albert B. Prescott Professor of Pharmaceutical Sciences, College of Pharmacy, University of Michigan, 428 Church Street, Ann Arbor, Michigan 48109-1065, Tel: (734)764-4273, Fax: (734)763-9772, vcyang@umich.edu.

The authors each declare no conflict of interest in this work.

Keywords

iron oxide nanoparticles; magnetic nanoparticles; magnetic targeting; polyethylene glycol (PEG); pharmacokinetics; reticuloendothelial system (RES); drug delivery; brain tumor; glioma

1. INTRODUCTION

In the United States, approximately 18,500 new cases of primary intracranial tumors are diagnosed annually [1]. The prognosis for those afflicted with a brain tumor is usually grim, with glioblastoma multiforme (the most common and most severe form of primary brain tumor) patients showing a median survival rate of just 9–12 months post-diagnosis [2]. The ideal remissive therapy for brain tumors will likely require a multi-functional approach that avoids the invasiveness/incompleteness of surgery and concurrently addresses the shortcomings of today's adjuvant chemo and radiation therapies. Magnetic iron oxide nanoparticles (MNPs) have been investigated in both brain tumor diagnostics (primarily in magnetic resonance imaging - MRI) and drug delivery [3–6]. These "theranostics" possess a high surface area-to-volume ratio, which provides for high loading capacity of functional cargoes that can include drugs, molecular targeting moieties, cell internalization agents, and/or pharmacokinetic stabilizers [7]. Indeed, the combination of anti-tumor drug(s) and functionalities that enhance drug efficacy onto a single platform could substantially improve therapeutic indices, even for macromolecular agents. In addition to targeting from the enhanced permeability and retention (EPR) effect and with tumor-specific molecular ligands, the magnetic responsiveness of MNPs to an external magnetic field can be used for "magnetic targeting" of nanoparticles to tumors [7–9]. Magnetic targeting is especially attractive for brain tumors as it is noninvasive and does not interfere with normal brain function.

Along with others, we have explored magnetic brain tumor targeting of MNPs extensively [10–15]. Considering the requirements for magnetic targeting, suitable MNPs generally possess larger cores (>100 nm) to ensure that sufficient magnetic force is generated on nanoparticles [16]. A larger particle size, however, can attenuate the residence time of MNPs in the circulation, effectively limiting nanoparticle exposure to the tumor [16]. For example, when 100 nm starch-coated MNPs were magnetically targeted to 9L-glioma brain tumors in rats after intravenous administration, less than 0.1% injected dose Fe/g tumor delivery was achieved [13]. The consequence of such inefficiency could necessitate dose escalations that increase the risk for off-target, drug-induced toxicity. Intracarotid injections (to immediately access the brain vasculature after dosing) [12] and focused ultrasound (FUS) [6] have been considered to improve targeting efficiency, yet do not directly address nanoparticle pharmacokinetics. Interestingly enough, the coupling of a long-circulating MNP to magnetic brain tumor targeting has not been well studied, likely due to the challenges of identifying a suitable nanoparticle formulation. Longer circulation times render MNPs better exposed to tumors [16] and could result in substantially better magnetic tumor targeting efficiency as shown in Figure 1.

To address limitations in magnetic targeting efficiency attributed to fast MNP circulation clearance, we recently developed a polyethylene glycol (PEG) modified, cross-linked starch coated MNP (PEG-MNP) that showed sustained exposure to tumors in 9L-glioma bearing rats [16]. While long-circulating, previous data indicated that PEG-MNPs are eventually cleared from the circulation [16]. MNPs are generally removed from the bloodstream by tissue macrophages of the reticuloendothelial system (RES), often resulting in a relatively high biodistribution in the liver (80–90% of dose) and the spleen (5–8% of dose) [17–22]. These and other organs of elimination are at especially high risk for off-target toxicity when

drug-loaded nanoparticles are administered and subsequently cleared from the bloodstream. Therefore, a thorough understanding of MNP distribution patterns in these tissues is critical when considering a specific nanoparticle platform for drug delivery. Such knowledge can also confirm differences in circulation pharmacokinetics observed between different MNPs and possibly give insight to route(s) of total body nanoparticle elimination.

This work first profiled biodistribution of PEG-MNPs in key organs of elimination (e.g. liver, spleen, lung, and kidney) throughout the course of their circulation clearance in a rat model. Comparisons were made with data obtained for a starch-coated MNP, the parent nanoparticle to PEG-MNPs and that used in our previous magnetic brain tumor targeting study discussed above. After evaluating the biodistribution patterns of PEG-MNPs in organs of elimination, we then sought to confirm that enhanced brain tumor delivery of these nanoparticles is achieved with magnetic targeting, due to their extended residence in circulation and improved tumor exposure. Proof-of-concept was realized in the 9L-glioma rat model used throughout our previous investigations, using the starch-coated MNP as a benchmark.

2. MATERIALS AND METHODS

2.1. Materials

All materials were obtained from commercial suppliers and used without further modification, unless otherwise noted. Starch-coated, fluidMAG-D (“D”) magnetite (Fe_3O_4) nanoparticles were purchased from Chemicell® GmbH (75 mg/mL, Berlin, Germany). *N*-hydroxysuccinimidyl (NHS) activated methoxyl polyethylene glycol succinimidyl carbonates (SC NHS-PEG), in 5 and 20 kDa molecular weights, were obtained from Nanocs (New York, NY). Dimethylsulfxodide (DMSO), sodium phosphate (mono- and di-basic), 37% hydrochloric acid (HCl), epichlorohydrin, concentrated ammonium hydroxide (NH_4OH, containing 30% ammonia), sodium hydroxide pellets (NaOH), potassium hexacyano-ferrate (II) trihydrate, nuclear fast red solution, and 10% neutral-buffered formalin solution were obtained from Sigma-Aldrich (St. Louis, MO). Ethanol (EtOH) preparations were obtained from Decon Labs (King of Prussia, PA). Xylenes and Permount tissue-mounting medium were obtained from Fisher Scientific (Waltham, MA). Dulbecco’s Modified Eagle Medium (DMEM – supplemented with L-glutamine and sodium pyruvate), antibiotics, heat inactivated fetal bovine serum (FBS), cell culture grade phosphate buffered saline (PBS—1X–pH 7.4), and 0.25% trypsin-EDTA were obtained from Invitrogen (Carlsbad, CA). Deinoized water (DI H_2O) used in syntheses and histological preparations was obtained from a Milli-Q A10 Biocel water purification system (Millipore, Billerica, MA). Rat 9L gliosarcoma cells were obtained from the Brain Tumor Research Center (University of California, San Francisco, CA). Bone wax was obtained from Ethicon (Somerville, NJ) and Vetbond tissue adhesive from 3M (St. Paul, MN). Sterile heparin and (10 U/mL and 5000 U/mL - Abraxis, Los Angeles, CA) 0.9% sodium chloride (Hospira, Lake Forrest, IL) injection solutions were obtained from the University of Michigan Hospital Pharmacy.

2.2. Synthesis of polyethylene glycol modified, cross-linked starch MNPs (D5 & D20 – “PEG MNPs”)

Cross-linked, aminated starch coated MNPs grafted with 5 kDa (“D5”) or 20 kDa (“D20”) molecular weight polyethylene glycol (PEG) were synthesized to produce PEG-MNP derivatives as previously described [16]. Briefly, 2 mL of D (42 mg Fe/mL) were incubated with 2.6 mL NaOH and 1.3 mL of epichlorohydrin for 24 hr at 25°C with shaking. After purification via dialysis against DI H_2O, the cross-linked starch MNP (DXL - ~12 mL) was then shaken with 2 mL of concentrated NH_4OH (30% ammonia) for 24 hr at 25°C. The

cross-linked, aminated product (DN) was obtained after purification by dialysis against DI H_2O. A Dynal magnetic separator (Invitrogen, Carlsbad, CA) was used to concentrate DN to approximately 30–40 mg Fe/mL. 320 μL of DN (30 mg Fe/mL) was then shaken with 320 μL DMSO and 0.1 M (pH 8) phosphate buffer (320 μL for D5, 640 μL for D20) containing ~30 mg of the appropriate SC NHS-PEG at 25°C for 3 hr. D5 and D20 were purified with four washes of DI H_2O via magnetic separation. Particle size was measured using dynamic light scattering (DLS) on a ZetaSizer Nano ZS90 instrument (Malvern, Worcestershire, UK) and controlled (to values similar to those previously reported [16]) with sonication using a Sonifier (Branson, Danbury, CT) sonicator operated at 10% amplitude at 25°C. Final suspensions were concentrated to approximately 40 mg Fe/mL using magnetic separation. Iron content of the various aforementioned MNP preparations was assessed with inductively coupled optical emission (ICP-OES) spectroscopy on an Optima DV 2000 spectrometer (Perkin Elmer, Waltham, MA) as previously described [16]. The key physical and pharmacokinetic properties of the two PEG-MNPs determined previously are shown in Table 1.

2.3. Biodistribution of PEG-MNPs in organs of elimination

All animal experiments were conducted according to protocols approved by the University of Michigan Committee on Use and Care of Animals (UCUCA).

Male Fisher 344 rats (~200 g, Harlan, Indianapolis, IN, n=3/MNP type) were anesthetized by intraperitoneal injection of a ketamine/xylazine mixture (87/13 mg/kg BW). The lateral tail vein was cannulated with a 26-gauge Angiocath™ catheter (Hospira, Lake Forrest, IL) and flushed briefly with 10 U/mL heparin lock solution. MNP suspensions were diluted to 10.25 mg Fe/mL in 1X cell culture grade PBS (pH 7.4) and administered through the catheter at a dose of 12 mg Fe/kg, consistent with pharmacokinetic analyses of D5 and D20 described previously [16]. 0.9% sodium chloride solution was used to flush residual nanoparticle suspension remaining in the catheter into the bloodstream after the initial MNP injection. At time-points of 1, 12, or 60 hr after administration, animals were anesthetized intraperitoneally with a ketamine/xylazine mixture (87/13 mg/kg) and euthanized by decapitation. Liver, spleen, lung, and kidney tissues were collected from euthanized animals and stored at −80°C for quantitative analysis (Section 2.7). D was studied at 1 hr for comparisons with PEG-MNPs. For animals exposed to PEG-MNPs, a ~100 mg tissue sample of each organ type was also obtained immediately after euthanasia for histological analysis described in Section 2.8.

2.4 Induction of 9L brain tumors in rats

Intracerebral brain tumors were induced in male Fisher 344 (125–150 g) rats as described elsewhere [23]. Briefly, 9L glioma cells were cultured to confluence in T75 flasks in DMEM medium containing 10% heat inactivated FBS, 1% antibiotics, and 0.29 mg L-glutamine at 37°C in a humidified atmosphere containing 5% CO_2. Immediately prior to initiation of surgery, cells were harvested using 0.25% trypsin-EDTA, washed twice with serum free medium, and each flask of cells suspended in ~1.3 mL serum free medium to a concentration on the order of 10^4 cells/μL. Animals were anesthetized by intraperitoneal injection of ketamine/xylazine mixture as described in Section 2.3. Following a small skin incision over the right hemisphere of the skull, a 1-mm-diameter burr hole was drilled into the skull approximately 1 mm anterior to the bregma and 5 mm lateral from the midline. 10 μL of 9L cell suspension was injected into the brain at a depth of 3–4 mm beneath the skull. To prevent extracerebral extension of the tumor, the surgical field was cleaned several times with 100% ethanol and the burr hole sealed with bone wax. The surgical site was then cleaned with an iodine scrub followed by closure of the skin incision with tissue adhesive. Animals were imaged every 2–3 days using a fast spin echo T_2-weighted MRI (see Section

2.6) sequence starting 11 days after tumor induction to select tumors between 50–100 μL in volume. Tumor volumes were assessed with in-house developed MATLAB software running sizing algorithms previously described [23].

2.5. Magnetic brain tumor targeting of MNPs

Animals (~200 g) possessing tumors of volume 50–100 μL were subject to a magnetic brain tumor targeting strategy described previously [12]. Animals were anesthetized with a ketamine/xylazine mixture (87/13 mg/kg) and tail catheterized as described in Section 2.3. They were then placed supinely in a tubular holder with an 11-mm diameter hole removed to expose the anterior right hemisphere of the animal head – the site of tumor implantation. Through the 11-mm hole, the animal head was placed directly on the pole face of a 9-mm diameter, cylindrical NdFeB magnet (Allstar Magnetics, Vancouver, WA) secured to one 40-mm diameter pole of a 3470 dipole electromagnet (GMW Associates, San Carlos, CA). The electromagnet was operated at 0.4 T at its pole faces (measured with a Hall Teslameter) to produce a magnetic field strength of approximately 0.2 T at the 9-mm magnet pole face. Following successful setup of the targeting apparatus, MNP suspensions (10.25 mg Fe/mL) were administered (12 mg Fe/kg) through the catheter and animals (n=5) retained in the magnetic field for 1 hr. Animals (n=4) injected with MNPs but not exposed to the magnetic field were used as a control for targeting. Anesthesia was maintained over the 1 hr targeting time with a subsequent dose of ketamine (29 mg/kg) at 30 min. At the conclusion of targeting (or 1 hr for control animals), animals were removed from the targeting apparatus, imaged with MRI (Section 2.6), and immediately euthanized by decapitation. A set of targeted/non-targeted animals was also imaged at several time points following targeting to visualize MNP clearance from tumors post-targeting. Intact brains were immediately removed from euthanized animals after opening of the skull. The brain was separated into hemispheres and entire tumors carefully dissected from their location in the right hemisphere. Excised normal brain (left hemisphere) and tumor tissues were stored at −80°C prior to quantitative analysis with ESR as described in Section 2.7. D was studied as a benchmark for comparison. Targeting (TA) and selectivity (SA) advantages were calculated from average tissue MNP concentrations according to Equations 1 and 2:

$$TA_{PEG-MNP} = \frac{[PEG-MNP]_{tumor,target}}{[MNP]_{tumor,benchmark}} \quad (1)$$

$$SA_{MNP} = \frac{[MNP]_{tumor}}{[MNP]_{brain}} \quad (2)$$

An additional set of targeted/non-targeted tumor and normal brain tissues was obtained for histological analysis for each nanoparticle administered. For these samples, tumor was not separated from the normal brain tissue and was processed as described in Section 2.8.

2.6. MRI monitoring of MNP delivery to brain tumors

MNP presence in tumor and normal brain was monitored by MRI as described elsewhere [16]. Images were acquired on a 30-cm horizontal-bore, 7T Direct Drive small animal imaging system (Agilent, Santa Clara, CA). Animals were anesthetized by inhalation of a 1.5% isoflurane/air mixture and imaged using a rat head quadrature RF coil (m2m Imaging, Cleveland, OH). Tumor positioning in the brain was visualized prior to MNP administration using a high resolution T_2-weighted fast spin echo sequence with the following parameters: repetition time (TR) = 4000 ms, echo time (TE) = 30 or 60 ms, field of view 30 × 30 over

256 × 128 matrix, slice thickness = 1 mm, slice separation = 0 mm, number of slices = 15, and two signal averages. Real time visualization of MNP presence in the normal brain and tumor was achieved using a T_2*-weighted gradient echo (GE) sequence set with the following parameters: TR = 180 ms, TE = 5 ms, flip angle = 20 deg, field of view = 30 × 30 over 128 × 128 matrix, slice thickness = 1 mm, slice separation = 0 mm, number of slices = 15, and one signal average. Baseline T_2-weighted and GE images were taken sequentially without animal repositioning. GE MR images were obtained immediately and at later time points after magnetic targeting to visualize both the success of targeting and nature of nanoparticle clearance from tumors after removal of the magnetic field respectively. Animals were repositioned in the magnet between imaging time points, with the T_2-weighted slice showing the best cross-sectional view of the tumor at baseline used to select corresponding GE images at later time points.

2.7 *Ex vivo* analysis of tissue MNP content with electron spin resonance spectroscopy (ESR)

MNP concentrations in excised tissues (Section 2.3 and 2.5) were quantitatively evaluated using electron spin resonance (ESR) spectroscopy as described previously [22]. Briefly, ESR spectra were acquired using an EMX ESR spectrometer (Bruker, Billerica, MA) operated at: resonant frequency = ~9.2 GHz; microwave power = 20 mW; and temperature = −128°C. The combination of receiver gain and modulation amplitude settings varied by tissue type and MNP studied as displayed in Table 2. Frozen organs were sectioned into approximately 2 mm × 2 mm × 2 mm cubes with a razor blade, applied to the top of an ESR tube, and quickly pushed to the bottom of the tube using a glass rod [22]. For biodistribution studies, ~30 mg of tissue was loaded into each tube, in triplicate for each organ sample collected (e.g. n=9; 3 cuts × 3 animals studied). For brain tumor targeting studies, ~30 mg of normal brain tissue was loaded into each tube, in triplicate for each organ sample collected (e.g. n=12–15; 3 cuts × 4–5 animals studied). The entire excised tumor (~45–65 mg) in was loaded into a single ESR tube, due to the limited amount of tissue available. MNP suspensions of known-iron-concentration were utilized as calibration standards. Spectra were obtained as the first derivative (dP/dB) of absorbed microwave power (P) vs. the applied magnetic field (B). It is known that the double integral (DI) of collected spectra ($\iint (dP/dB)dBdB$) is proportional to the number of resonating electronic spins in a measured sample. DI values, used to determine tissue MNP content and construct calibration curves from MNP standards, were calculated from obtained spectra using WinEPR software (Bruker, Billerica, MA). For all tissues studied, blank tissues showed negligible signal compared to those exposed to MNPs, and, therefore, background correction was not required. Tissue iron amounts were normalized by weight and averaged to obtain tissue MNP concentrations (nmol Fe/g tissue) for each type of organ/MNP combination studied.

2.8. *Ex vivo* histological analysis of MNP localization in excised tissues

Tissue samples obtained for histology were immediately immersed in 10% neutral-buffered formalin solution for 24 hr following excision. After fixation, tissues were stored in 70% EtOH for further processing. Stored tissues were dehydrated through 100% EtOH, exposed to xylene, and internally embedded with paraffin wax using an ASP 300 Tissue Processor (Leica, Wetzlar, Germany). Processed tissues were then encased in paraffin blocks using an EG1160 embedding center (Leica, Wetzlar, Germany). 5 μm tissue sections were cut from paraffin blocks using a Leica RM 2155 Microtome and subsequently affixed to Superfrost microscopy slides (Fisher Scientific, Waltham, MA). Prussian Blue staining is a highly sensitive method for identifying ferric species in tissues and was used with a nuclear fast red counterstain to visualize MNP content in obtained tissue sections [17, 24–26]. Briefly, microscopy slides containing tissue sections were sequentially immersed in xylene to dissolve excess paraffin and rehydrated through immersion in decreasing concentrations

(100-70%) of EtOH in DI H_2O followed by 100% DI H_2O. Slides were then immersed in a freshly prepared solution containing equal parts 20% HCl and 10% potassium ferrocyanide for 20 min at 25°C. Iron stained slides were rinsed in DI H_2O and subsequently immersed in nuclear fast red solution for 5 min at 25°C. Slides were then rinsed in DI H_2O, dehydrated through increasing concentrations (80% – 100%) of EtOH, and cleared in xylene. Dehydrated tissues were coverslipped with Permount resinous mounting medium and allowed to dry overnight at ambient temperature. Stained slides were visualized and photographed with light microscopy at 10× and 40× magnification using a fixed-stage, upright E-800 light microscope (Nikon, Melville, NY) equipped with a 12.5 megapixel cooled CCD DP71 digital camera (Olympus, Center Valley, PA).

2.9. Statistical analyses

All data are presented as mean ± standard deviation. Statistical comparisons made in both biodistribution and magnetic brain tumor targeting studies were made using the Student's *t* test with a significance of $p < 0.05$.

3. RESULTS

3.1. Biodistribution of PEG-MNPs in organs of elimination

3.1.1. Biodistribution of D & PEG-MNPs in liver and spleen at 1 hr—To confirm the observed differences in plasma pharmacokinetic behavior reported previously [16] and initially assess any key differences in biodistribution patterns between D and PEG-MNPs, nanoparticle biodistribution was studied in liver and spleen 1 hr after MNP administration. A 1 hr time point was chosen as previous data for D suggested this to be sufficient time for complete clearance of D from the circulation at the studied dose (12 mg Fe/kg). As shown in Figure 2, D is similarly concentrated to a fairly high extent in both the liver (3150 ± 460 nmol Fe/g tissue) and spleen (3670 ± 610 nmol Fe/g tissue) following its removal from the circulation. In stark contrast, tissue concentrations of D5 (251 ± 41 nmol Fe/g tissue) and D20 (278 ± 31 nmol Fe/g tissue) in the liver were 11.3–12.5-fold lower at 1 hr. Spleen concentrations of D5 (1700 ± 420 nmol Fe/g tissue) and D20 (1360 ± 390 nmol Fe/g tissue) were also lower, presenting values 2.2–2.6-fold lower than those obtained with D. Data indicate that both PEG-MNPs are distributed to a statistically ($p < 0.0001$) lower extent in these two tissues than is D at 1 hr.

3.1.2. Time course of PEG-MNP biodistribution in organs of elimination—After confirming that distributions of both PEG-MNPs were indeed lower in the liver and spleen compared to cleared parent D at 1 hr, we examined the longer-term distribution patterns of these nanoparticles in organs of elimination. In addition to tissue collection at 1 hr, time points of 12 and 60 hr were also collected as they represent a mid-range and final time point, respectively, of the plasma pharmacokinetic profiles reported previously [16]. The time course for each organ type is shown in Figure 3. Generally speaking, measured tissue concentrations of nanoparticles in lung are similar for both PEG-MNPs. At 1 hr, measurable lung MNP concentrations (D5 – 312 ± 98 nmol Fe/g tissue, D20 – 444 ± 80 nmol Fe/g tissue) were observed, more or less level off at 12 hr (D5 – 454 ± 110 nmol Fe/g tissue, D20 – 416 ± nmol Fe/g tissue), and have decreased by about 3-fold at 60 hr (D5 – 154 ± 52 nmol Fe/g tissue, D20 – 150 ± 52 nmol Fe/g tissue). Histology images (Figure 4), though, show that only very minute instances of Prussian Blue can be observed for either PEG-MNP in lung tissue (located primarily in the tissue interstitium, 40× inset box) at any of the studied time points, despite measurable nanoparticle levels in quantitative studies. Moreover, a similar discrepancy was observed in kidney. Measured kidney concentrations (Figure 3) of MNPs are highest at 1 hr (D5 – 150 ± 24 nmol Fe/g tissue, D20 – 173 ± 43 nmol Fe/g tissue), decrease by 2–3 fold at 12 hr (D5 – 75 ± 9 nmol Fe/g tissue, D20 – 59 ± 16 nmol Fe/

g tissue), and decline further through 60 hr (D5 – 18 ± 9 nmol Fe/g tissue, D20 – 31 ± 13 nmol Fe/g tissue). Kidney micrographs (Figure 4) for both PEG-MNPs at all time points collected are nearly identical to those obtained from blank tissues, though, with no observable Prussian Blue in tissue spaces.

In the liver, biodistribution profiles are nearly identical for both PEG-MNPs. A small increase in tissue MNP concentration can be observed for both D5 (to 505 ± 117 nmol Fe/g tissue) and D20 (to 545 ± 79 nmol Fe/g tissue) at 12 hr with concentrations somewhat lower (D5 – 335 ± 42 nmol Fe/g tissue, D20 – 372 ± 68 nmol Fe/g tissue) at 60 hr. Throughout the time course studied, measured tissue concentrations of PEG-MNPs remained substantially lower than that obtained for D at 1 hr (Figure 2). Little Prussian Blue can be observed in liver tissue micrographs at 1 hr (Figure 4), similar to images of blank tissues not exposed to MNPs. Small areas of Prussian Blue, though, can be observed in liver (40× inset images in Figure 4) at 12 and 60 hr. These regions of limited MNP accumulation appear to be localized primarily in the hepatic sinusoids, the primary location of phagocytic Kupffer cell macrophages typically responsible for MNP clearance [19, 27].

Compared to observations in kidney, lung, and even liver, results are markedly different in the spleen. As shown in Figure 3, measured spleen concentrations of both D5 (4620 ± 710 nmol Fe/g tissue) and D20 (7410 ± 950 nmol Fe/g tissue) are 2.7–5.4-fold higher, respectively, than measurements for each MNP obtained at 1 hr (Figures 2 & 3). Spleen MNP concentrations increase to even greater values at 60 hr (D5 – 6650 nmol ± 1690 nmol Fe/g tissue, D20 – 8680 ± 820 nmol Fe/g tissue). Undoubtedly, tissue concentrations for both PEG-MNPs are substantially higher at 12 and 60 hr time points when compared to measurements taken at 1 hr for spleen exposed to parent D or either PEG-MNP (Figure 2). Histological analyses of spleen tissues in Figure 4 generally agree with quantitative data shown in Figure 3. As the spleen is the primary site for destruction of old red blood cells and subsequent recycling of hemoglobin bound iron, Prussian Blue deposits can be observed in the red pulp regions of blank spleen tissues [28]. The size and intensity of individual Prussian Blue deposits in the red pulp increase over the 60 hr time course. Furthermore, the size and intensity of Prussian Blue deposits in D20 (Figure 4B) exposed tissues appear to be greater than those observed in tissues exposed to D5 (Figure 4A), consistent with *ex vivo* data that suggest higher concentrations of D20 in spleen tissue at later time points (Figure 3).

3.2. Magnetic brain tumor targeting of PEG-MNPs

As mentioned above, we previously targeted D in 9L-glioma bearing rats at a dose of 12 mg Fe/kg [13]. The animal model and dose were useful in that study and, thus, also used for this investigation. A targeting time of 1 hr was chosen as it reasonably coincided with the total circulation lifetime (and, thus, expected tumor exposure) of D reported previously, at the given dose [16]. Comparisons with PEG-MNPs targeted for the same time provided a good means to substantiate enhanced brain tumor targeting of nanoparticles.

3.2.1. Proof-of-concept: enhanced magnetic brain tumor targeting of PEG-MNPs—MRI, quantitative ESR analysis of extracted tissues, and histology were all used to verify enhanced magnetic brain tumor targeting of PEG-MNPs. The MNP induced changes in T_2-weighted MR image hypointensity provide real time information about nanoparticle delivery to tissues, including tumor-bearing brains [13, 16]. MR images of magnetically targeted/non-targeted D, D5, and D20 are shown in Figure 5, immediately following the completion of targeting (or 1 hr for control animals). In baseline T_2-weighted fast spin echo scans (T_2-0), the positioning of the tumor in the brain is clearly visible as a hyperintense region located on the right side of the brain. Prior to administration of MNPs, baseline T_2*-

weighted GE scans (GE-0) show no hypointensity in either the tumor or normal brain regions, indicated by the lack of contrast in both tissues. After administration of MNPs and passive (no targeting) delivery of PEG-MNPs to tissues over 1 hr, however, contrast can be observed as hypointense regions in both normal brain and tumor tissues on GE images (GE-1). Tumor regions have considerably less signal than normal brain tissues, consistent with results obtained previously [16]. In contrast, GE images obtained from animals exposed to D for 1 hr are similar to those obtained at baseline with little detectable change in hypointensity. Pronounced tumor signal reduction, though, can be observed for all three MNPs studied with the inclusion of the external magnetic field. As shown in Figure 5, magnetically targeted tumors exposed to each type of MNP show increased hypointensity in the tumor region when compared to controls. Similarity between normal brain tissues exposed to each type of MNP also exists, with no visibly distinguishable difference in tissue contrast between images obtained from targeted and non-targeted animals. The contrast intensity of tumors targeted with PEG-MNPs, however, is dramatically greater than that observed in images of targeted tumors exposed to D. In fact, the observed hypointensity of targeted tumors exposed to D5 and D20 is so dark that it is visually impossible to discern any differences in contrast between the two nanoparticles. Moreover, observed contrast in non-targeted tumors exposed to PEG-MNPs also appears to be greater when compared to those targeted with D. It should be noted that, because of such significant signal loss in both targeted and non-targeted tumors exposed to either PEG-MNP, quantitative information typically extracted from regions-of-interest (ROIs) drawn over the tumor could not be accurately calculated from the obtained images.

Quantitative information obtained from integrations of ESR spectra is shown in Figure 6. Tumor MNP concentrations are higher after targeting for PEG-MNPs, with targeted D5 (345 ± 70 nmol Fe/g tissue) and D20 (429 ± 113 nmol Fe/g tissue) tissues showing statistically higher ($p<0.005$) MNP concentrations than their non-targeted counterparts (D5 – 69 ± 18 nmol Fe/g tissue, D20 – 77 nmol ± 15 nmol Fe/g tissue). The longer circulating D20 did have a higher average tumor concentration than D5, but the results were not statistically different ($p=0.20$). Still, though, observed delivery of D5 and D20 in targeted tumors represents approximately 0.8% and 1.0% of injected dose/g tissue, respectively. Results for D were similar in pattern, with targeted tumors exhibiting greater tissue MNP concentration (29 ± 13 nmol Fe/g tissue) than those non-targeted (1.9 ± 0.4 nmol Fe/g tissue). D exposed tumors, though, possessed statistically ($p<0.005$) lower MNP concentrations compared to those exposed to either PEG-MNP, with determined values for targeted tissues representing 0.07 % injected dose/g tissue – a targeting efficiency consistent with our previous study evaluating D [13]. To quantify targeting enhancements over several benchmarks (non-targeted PEG-MNP, targeted D, and non-targeted D), TA values were calculated according to Equation 1 and are displayed in Table 3. In normal brain, concentrations of D5 (targeting – 13 ± 8 nmol Fe/g tissue, no targeting – 12 ± 7 nmol Fe/g tissue), D20 (targeting – 15 ± 8 nmol Fe/g tissue, no targeting – 16 ± 7 nmol Fe/g tissue), and D (targeting – 1.8 ± 0.6 nmol Fe/g tissue, no targeting – 1.7 ± 0.3 nmol Fe/g tissue) were low and not statistically different for each type of MNP with and without targeting. Normal brain tissue levels of D5 or D20, though, were somewhat higher than those observed for D. Tumor SA values were calculated (Table 4) according to Equation 2 to contextualize enhancements in tumor MNP selectivity over normal brain from the addition of magnetic targeting. SA values increased with the addition of magnetic targeting and are about twice as high for PEG-MNPs over D.

Histological data shown in Figure 7 qualitatively complements data obtained with MRI and ESR. Tumors exposed to D are similar with a very small amount of Prussian Blue (single region shown in 10× and 40× images) detected in the targeted tumor and no detectable Prussian Blue in the control. For PEG-MNPs, however, a number of heterogeneously distributed regions of Prussian Blue deposition are easily seen in tumors at both 10 and 40×

magnification, with the largest in size appearing near the tumor/brain boundary. Smaller deposits of Prussian Blue were also observed throughout the bulk of the tumor lesion (data not shown). Despite showing strong contrast in MR images and measurable levels with ESR, though, Prussian Blue was detected in non-targeted tumors to a smaller than expected extent after administration of D20 and not at all in tissues exposed to D5, suggesting limited passive retention. With respect to selectivity, Prussian Blue depositions appear to be confined to the tumor space, with no Prussian Blue detected in the normal brain both near the tumor/normal brain interface (shown in tumor images) and in the bulk tissue regardless of the MNP administered or inclusion of the external magnetic field.

3.2.2. Visualizing post-targeting tumor clearance of PEG-MNPs with MRI—A GE MRI time course (Figure 8) was used to gain insight into the post-targeting tumor clearance of PEG-MNPs and compare observed behavior with parent D. MR images of D generally agree with previously obtained data [13], as targeted tumors do show similar levels of hypointensity at 1 and 3 hr, after which it becomes less detectable [13]. In the case of PEG-MNPs, Figure 5 shows that tumor hypointensity is greater immediately after targeting when compared to non-targeted tissues. Following hypointensity over time (Figure 8), however, it is clear that nanoparticles steadily clear from the tumor soon after targeting. Hypointensity of tumors is noticeably less at 3 hr and continues to drop throughout the imaged time course. Images appear to suggest that post-targeting tumor clearance is relatively quick for PEG-MNPs when compared to previously targeted parent D.

4. DISCUSSION

Considering first our biodistribution results, it is not surprising that kidney levels of PEG-MNPs remain low throughout the tested time course in light of results obtained for D previously [22] and the larger size of the nanoparticles. Considering the steadily decreasing tissue MNP concentrations (Figure 3) over the tested time course and histology micrographs (Figure 4), it is likely that much of the ESR determined MNP content in kidney is localized to tissue blood (still containing measurable levels of MNPs) that washes away during histology preparation. Such behavior might also occur in the lung where the pattern is similar.

Indeed, an interesting find of this study is the unusual distribution profiles of PEG-MNPs observed in the liver and spleen. Tissue concentrations of both PEG-MNPs studied are at reduced levels in the spleen and liver (Figure 2) when compared to parent D at 1 hr. The data in Figure 2 corroborate pharmacokinetic data reported previously, as lower liver and spleen levels of nanoparticles imply that PEG-MNPs resist RES clearance and remain, instead, in circulation. Also, the lack of proportional reductions in tissue PEG-MNP concentrations between spleen (2.2–2.6-fold reduction) and liver (11.3–12.5-fold reduction) provides initial evidence that PEG-MNPs avoid liver distribution somewhat and are, instead, sequestered to an enhanced extent in the spleen. Moreover, liver PEG-MNP concentrations remain substantially lower than those observed for D at 1 hr (Figure 2), throughout plasma clearance (Figure 3). Histology data (Figure 4) do show distribution of MNPs in the liver at 12 and 60 hr, yet micrographs do not look substantially different between time-points suggesting a limited distribution. In short, results suggest that the liver does participate in the clearance of nanoparticles from the circulation, but in a reduced capacity compared to its more prominent role in clearing many other studied MNPs from the circulation. Reduced delivery of MNPs to the liver could be advantageous, as the tissue can be a key site of off-target, drug induced damage due to its function as the main site of detoxification in the body [29]. Even where a therapeutic might not cause toxicity when given as a “naked” (no modifications) formulation, toxicity could arise from substantial elevation in local concentrations caused by the accumulation of MNPs, each ideally attached to many copies

of a particular drug(s) [7]. Therefore, a mechanism that reduces exposure of the liver to MNPs might also help better minimize the risk for associated, drug-induced toxicity.

In contrast to the liver, both quantitative (Figure 3) and histological (Figure 4) time-courses show increasing PEG-MNP accumulations in the spleen, with measured nanoparticle concentrations at later time points markedly higher than those observed for D at 1 hr (Figure 2). Several plausible scenarios exist and might work in concert to produce the unexpected distribution profiles of PEG-MNPs observed between liver and spleen. First, kinetics could play a role, in that, due to PEGylation, sterics substantially reduce liver macrophage ability to phagocytose MNPs. Over time, slower, but more capable, processes in the spleen are better able to remove nanoparticles from the circulation resulting in the increased tissue concentrations observed. Second, it could be that nanoparticles do gain size in the plasma over time—it is known that nanoparticles >200 nm are generally better cleared by the spleen [19]. Additionally, the differences in spleen concentrations between D5 and D20 might be explained by the longer PEG chain-length of D20, which could prevent tissue processes that begin to breakdown MNPs and result in greater spleen accumulations. Alternatively, D5 could distribute to a greater extent in tissues not studied. Elucidating the role of these potential mechanisms and the extent of their influence on increased spleen distribution and differences with respect to PEG size, however, requires further investigation. Regardless of the mechanisms responsible, though, elevated levels of PEG-MNPs in the spleen pose increased concerns for toxicity. As a result, additional biodistribution studies over the course of a longer time interval are necessary to understand the rate and extent of nanoparticle elimination from the spleen, and even the liver. Information obtained from these studies and assessment of tissues not studied would be useful in gaining a more complete picture of toxicity risks, the desired insight to routes of total body elimination of PEG-MNPs, and a better grasp on appropriate dosing regimens.

Shifting our focus, the results presented herein provide strong evidence that improved duration of lesion exposure to nanoparticles results in enhanced magnetic brain tumor targeting of PEG-MNPs. The targeting strategy utilized involved very little preparative work beyond creating an intravenous administration site and placing the animal head on the magnet. Clearly, our targeting setup could easily be translated to humans, assuming a magnet of sufficient strength was used. MR images obtained immediately following magnetic targeting provide the first pieces of evidence supporting enhanced delivery of PEG-MNPs. Figure 5 indicates that tumors targeted with PEG-MNPs possess greater contrast after targeting compared to tumors not exposed to the magnetic field or those targeted with D. The difference in observed tissue contrast is substantial between the “black” tumors targeted with each PEG-MNP and that that is only faintly hypointense, targeted with D. The data both qualitatively confirm the feasibility of magnetic brain tumor targeting and show that the strategy is more efficient when targeting a long-circulating PEG-MNP. Additionally, the level of contrast observed in normal brain between targeted and non-targeted tissues appears similar, suggesting that selectivity was not compromised when targeting a PEG-MNP. It is true that contrast can be observed in the normal brain of animals administered with either PEG-MNP. Due to the relatively long exposure of PEG-MNPs to tissue vasculature, magnetic susceptibility effects that extend some distance away from blood vessels are the likely cause of this hypointensity in the normal brain.

Quantitative analyses (Figure 6) of tumor and normal brain tissues quantitatively corroborate MR images, providing a second piece of evidence for proof-of-concept. TA values (Table 3), calculated to characterize enhancements in delivery of PEG-MNPs to tumors over several different benchmarks, help contextualize targeting improvements. Considering only the effect of targeting, a 5–5.5-fold improvement in tumor PEG-MNP concentration is observed after magnetic targeting. Considering the effect of long-circulating behavior, a 12–

15-fold increase in tumor concentration of targeted PEG-MNPs is observed over targeted D. When considering the effects of both strategies combined, the advantage is far more dramatic, with targeted PEG-MNPs showing a 184–229-fold advantage over passively delivered D. Quantitative results also confirm the observed selectivity in MR images. The addition of targeting does not result in statistically higher determined MNP content in the normal brain for any of the nanoparticles studied. In fact, due to the delivery enhancements from targeting, tumor selectivity over normal brain is enhanced for PEG-MNPs, as calculated by the SA values shown in Table 4. One likely source of this selectivity is the difference in blood flow rates between tumor and normal brain. Slower tumor flow results in reduced hydrodynamic drag force and, thus, reduced magnetic force needed to capture MNPs [10, 14]. The opposite is true in normal brain, where higher flows result in higher magnetic forces needed to capture nanoparticles. Thus, reduced effectiveness of the applied magnetic force in normal brain actually results in desired selectivity.

Histological data (Figure 7) obtained from tumor and normal brain tissues provides both further evidence for proof-of-concept and some insight to the degree of passive MNP retention. Tissue micrographs confirm that tumor localization of Prussian Blue attributed to targeted PEG-MNPs is higher than those for D and further demonstrate the observed tumor selectivity observed with MRI and ESR – all Prussian Blue is contained to tumor tissue, even at tumor/normal brain boundaries. The lack of Prussian Blue in normal brain tissues indicates that the small levels of MNPs detected with ESR are likely localized to the tissue blood as described above for lung and kidney tissues. The heterogeneous distribution of nanoparticle deposits observed in tumor was expected due to the variable density of tissue vasculature, diffusion limitations of MNPs in the tumor interstitium, and the intermittent permeability of the blood-tumor-boundary (BTB) characteristic of a solid brain tumor [7, 30]. An unexpected result of this study, however, was that tissue micrographs of non-targeted tumors show very limited PEG-MNP accumulation via passive mechanisms, despite the pronounced hypointensity observed in tumor MR images in Figure 5. As discussed above, no Prussian Blue could be observed for non-targeted tissues exposed to D5, suggesting that hypointensity shown in MR images and MNPs detected with ESR are primarily due to MNP localization in tumor vasculature or due to transient nanoparticle extravasation. Some Prussian Blue can be observed for D20, but this is fairly limited. The increased size of nanoparticles likely makes their passive penetration and diffusion into the tumor tissue more difficult and, thus, provides one possible explanation for the reduced (or lack of) deposition observed in tumors. The longer half-life of D20 increases the probability for tissue extravasation, however, and could be an explanation for the small, observed differences between D5 and D20 exposed tissues. In short, data conclusively indicate both the limited contribution of passive mechanisms to MNP targeting and the importance of magnetic force in both the capture of nanoparticles from the circulation and their subsequent retention.

The non-invasive, real-time capabilities of MRI also rendered it a good means by which to qualitatively assess the longer-term tumor retention of MNPs post-targeting, which could be required for sufficient drug action. It is evident from images in Figure 8 that a substantial reduction in tumor hypointensity of PEG-MNP targeted tumors is observed at 3 hr, suggesting that nanoparticles begin clearance soon after removal of the magnetic field. Indeed, tumors at this time point appear similar to non-targeted tumors in Figure 5 and MR images obtained previously [16]. In contrast, similar levels of contrast are observed in tumors targeted with D immediately after targeting and at 3 hr. The colloidal stability of parent D is likely limited *in vivo* and could actually help in its retention in tumors after targeting. As magnetically targeted nanoparticles come closer together, colloidal instability results in nanoparticle aggregation. Due to increased nanoparticle size, nanoparticles are trapped and their tissue clearance becomes impeded. The result is a more gradual reduction

in tumor hypointensity as depicted in Figure 8. Due to their PEGylated, cross-linked starch coat, however, the colloidal stability of PEG-MNPs is greatly enhanced. Just as PEG chains sterically resist mechanisms responsible for RES clearance, they also stabilize MNPs and prevent agglomeration. Where larger nanoparticle aggregates form *during* magnetic targeting and are retained (via increased size *and* magnetic force), demagnetized aggregates re-disperse into individual particles that are cleared from the tumor after targeting. Enhanced colloidal stability of PEG-MNPs could also further explain their limited, passive retention seen in histological micrographs of non-targeted tumors discussed above. Molecular targeting ligands could offer one solution to improving retention after magnetic targeting.

Still, our brain tumor targeting results are exciting. In the case of D20, 1.0% injected dose/g tissue was achieved, representing a substantial improvement over our previous studies with intravenously administered D (0.07% injected dose/g tissue). The obtained result is also about twice as high as that (0.5% injected dose/g tissue) achieved with an intracarotidly administered polyethylenimine (PEI)-coated MNP we recently explored as an alternative [12]. It is important to note that this work only considered a single PEG-MNP dose, targeted for a relatively short duration, using one particular magnet setup. Each of these parameters and the sub-parameters that comprise them could all be optimized to produce the best possible strategy. An especially important consideration is the possibility to target for longer than 1 hr, considering the long plasma half-lives of PEG-MNPs reported previously [16]. Moreover, other methodologies (e.g. FUS) developed to selectively improve the permeability of the BTB could be coupled with the targeting strategy used here to achieve even better, more homogeneous MNP delivery. Nevertheless, the coupling of our long-circulating PEG-MNPs to magnetic targeting appears to offer another promising step toward the development of an MNP-based therapy for brain tumors.

5. CONCLUSION

Biodistribution data confirm plasma pharmacokinetic results obtained previously and suggest that the liver is distributed with PEG-MNPs to a lesser extent when compared to many other studied MNPs, which could help reduce associated liver toxicity from drug-loaded nanoparticles. The spleen, however, showed enhanced distribution and sustained accumulation of PEG-MNPs, raising concerns for potential toxicity – longer studies, though, are needed to better assess such risk. Moreover, selective, enhanced brain tumor targeting of an intravenously administered PEG-MNPs was confirmed in a 9L-glioma rat model. Tumor delivery of up to 1.0% injected dose Fe/g tissue was observed, representing a 15 fold improvement in targeting efficiency over previously targeted parent D (0.07% injected dose/g tissue) at the given dose. Data also indicate a limited contribution of passive mechanisms to PEG-MNP retention in tumors, underscoring the importance of the inclusion of magnetic targeting (and possibly other targeting functionalities, such as tumor-specific ligands) to retention of the nanoparticles studied. Targeting results, though, are promising and warrant both the further development of drug loaded PEG-MNPs and concurrent optimization of the magnetic targeting strategy utilized.

Acknowledgments

This work was supported in part by National Institutes of Health (NIH) R01 Grants CA114612, NS066945, and a Hartwell Foundation Biomedical Research Award. This work was also partially sponsored by Grant R31-2008-000-10103-01 from the World Class University (WCU) project of South Korea and by the National Basic Research Program of China (973 Program) 2007CB935800. Victor C. Yang is currently a participating faculty member in the Department of Molecular Medicine and Biopharmaceutical Sciences, Seoul National University, South Korea. Adam Cole is the recipient of a NIH Pharmacological Sciences and Bio-related Chemistry Training Grant (GM007767 from NIGMS), a University of Michigan Rackham Pre-Doctoral Fellowship, and is currently an American Foundation for Pharmaceutical Education (AFPE) Pre-Doctoral Fellow. The authors would like to thank Amanda Welton of the UM Center for Molecular Imaging for additional animal suggestions and

technical assistance with MRI and Jeff Harrison of the UM Morphology Core for assistance with histological studies.

REFERENCES

1. Sanai N, Berger MS. Intraoperative stimulation techniques for functional pathway preservation and glioma resection. Neurosurg Focus. 2010; 28:E1. [PubMed: 20121436]
2. Sathornsumetee S, Reardon DA, Desjardins A, Quinn JA, Vredenburgh JJ, Rich JN. Molecularly targeted therapy for malignant glioma. Cancer. 2007; 110:13–24. [PubMed: 17520692]
3. Agrawal A, Min DH, Singh N, Zhu HH, Birjiniuk A, von Maltzahn G, et al. Functional delivery of siRNA in mice using dendriworms. ACS Nano. 2009; 3:2495–2504. [PubMed: 19673534]
4. Hadjipanayis CG, Machaidze R, Kaluzova M, Wang LY, Schuette AJ, Chen HW, et al. EGFRvIII antibody-conjugated iron oxide nanoparticles for magnetic resonance imaging-guided convection-enhanced delivery and targeted therapy of glioblastoma. Cancer Res. 2010; 70:6303–6312. [PubMed: 20647323]
5. Veiseh O, Sun C, Fang C, Bhattarai N, Gunn J, Kievit F, et al. Specific targeting of brain tumors with an optical/magnetic resonance imaging nanoprobe across the blood-brain barrier. Cancer Res. 2009; 69:6200–6207. [PubMed: 19638572]
6. Liu HL, Hua MY, Yang HW, Huang CY, Chu PC, Wu JS, et al. Magnetic resonance monitoring of focused ultrasound/magnetic nanoparticle targeting delivery of therapeutic agents to the brain. Proc Natl Acad Sci U S A. 2010; 107:15205–15210. [PubMed: 20696897]
7. Cole AJ, Yang VC, David AE. Cancer theranostics: the rise of targeted magnetic nanoparticles. Trends Biotechnol. 2011 In Press.
8. Pankhurst QA, Connolly J, Jones SK, Dobson J. Applications of magnetic nanoparticles in biomedicine. J Phys D-Appl Phys. 2003; 36:R167–R181.
9. Dobson J. Magnetic nanoparticles for drug delivery. Drug Dev Res. 2006; 67:55–60.
10. Chertok B, David AE, Huang Y, Yang VC. Glioma selectivity of magnetically targeted nanoparticles: a role of abnormal tumor hydrodynamics. J Control Release. 2007; 122:315–323. [PubMed: 17628157]
11. Chertok B, David AE, Moffat BA, Yang VC. Substantiating in vivo magnetic brain tumor targeting of cationic iron oxide nanocarriers via adsorptive surface masking. Biomaterials. 2009; 30:6780–6787. [PubMed: 19782394]
12. Chertok B, David AE, Yang VC. Polyethyleneimine-modified iron oxide nanoparticles for brain tumor drug delivery using magnetic targeting and intracarotid administration. Biomaterials. 2010; 31:6317–6324. [PubMed: 20494439]
13. Chertok B, Moffat BA, David AE, Yu FQ, Bergemann C, Ross BD, et al. Iron oxide nanoparticles as a drug delivery vehicle for MRI monitored magnetic targeting of brain tumors. Biomaterials. 2008; 29:487–496. [PubMed: 17964647]
14. David AE, Cole AJ, Chertok B, Park YS, Yang VC. A combined theoretical and in vitro modeling approach for predicting the magnetic capture and retention of magnetic nanoparticles in vivo. J Control Release. 2011 In Press.
15. Zhang L, Yu FQ, Cole AJ, Chertok B, David AE, Wang JK, et al. Gum arabic-coated magnetic nanoparticles for potential application in simultaneous magnetic targeting and tumor imaging. Aaps J. 2009; 11:693–699. [PubMed: 19842043]
16. Cole AJ, David AE, Wang J, Galban CJ, Hill HL, Yang VC. Polyethylene glycol modified, cross-linked starch coated iron oxide nanoparticles for enhanced magnetic tumor targeting. Biomaterials. 2011; 32:2183–2193. [PubMed: 21176955]
17. Lee MJ-E, Veiseh O, Bhattarai N, Sun C, Hansen SJ, Ditzler S, et al. Rapid pharmacokinetic and biodistribution studies using cholorotoxin-conjugated iron oxide nanoparticles: a novel non-radioactive method. PLoS ONE. 2010; 5:e9536. [PubMed: 20209054]
18. Jain TK, Reddy MK, Morales MA, Leslie-Pelecky DL, Labhasetwar V. Biodistribution, clearance, and biocompatibility of iron oxide magnetic nanoparticles in rats. Mol Pharm. 2008; 5:316–327. [PubMed: 18217714]

19. Gupta AK, Wells S. Surface-modified superparamagnetic nanoparticles for drug delivery: preparation, characterization, and cytotoxicity studies. IEEE Trans Nanobiosci. 2004; 3:66–73.
20. Medarova Z, Pham W, Farrar C, Petkova V, Moore A. In vivo imaging of siRNA delivery and silencing in tumors. Nat Med. 2007; 13:372–377. [PubMed: 17322898]
21. Goya GF, Grazu V, Ibarra MR. Magnetic nanoparticles for cancer therapy. Curr Nanosci. 2008; 4:1–16.
22. Chertok B, Cole AJ, David AE, Yang VC. Comparison of electron spin resonance spectroscopy and inductively-coupled plasma optical emission spectroscopy for biodistribution analysis of iron-oxide nanoparticles. Mol Pharm. 2010; 7:375–385. [PubMed: 20039679]
23. Ross BD, Zhao YJ, Neal ER, Stegman LD, Ercolani M, Ben-Yoseph O, et al. Contributions of cell kill and posttreatment tumor growth rates to the repopulation of intracerebral 9L tumors after chemotherapy: An MRI study. Proc Natl Acad Sci U S A. 1998; 95:7012–7017. [PubMed: 9618530]
24. IHCWorld.com. Prussian blue staining protocol for iron. 2010 August. Online. Available from URL: http://www.ihcworld.com/_protocols/special_stains/prussian_blue.htm
25. Carson, FL. Histotechnology: a self-instructional text. Chicago: ASCP Press; 1997.
26. Huang B-R, Chen P-Y, Huang C-Y, Jung S-M, Ma Y-H, Wu T, et al. Bioavailability of magnetic nanoparticles to the brain. J Magn Magn Mater. 2009; 321:1604–1609.
27. McCuskey RS, McCuskey PA, Urbaschek R, Urbaschek B. Kupffer cell-function in host defense. Rev Infect Dis. 1987; 9:S616–S619. [PubMed: 3317754]
28. Bowdler, A. The Complete Spleen: Structure, Function, and Clinical Disorders. Totowa: Humana Press; 2002.
29. Senior JR. Unintended hepatic adverse events associated with cancer chemotherapy. Toxicol Pathol. 2010; 38:142–147. [PubMed: 19858501]
30. Lampson LA. Targeted therapy for neuro-oncology: reviewing the menu. Drug Discov Today. 2009; 14:185–191. [PubMed: 19063992]

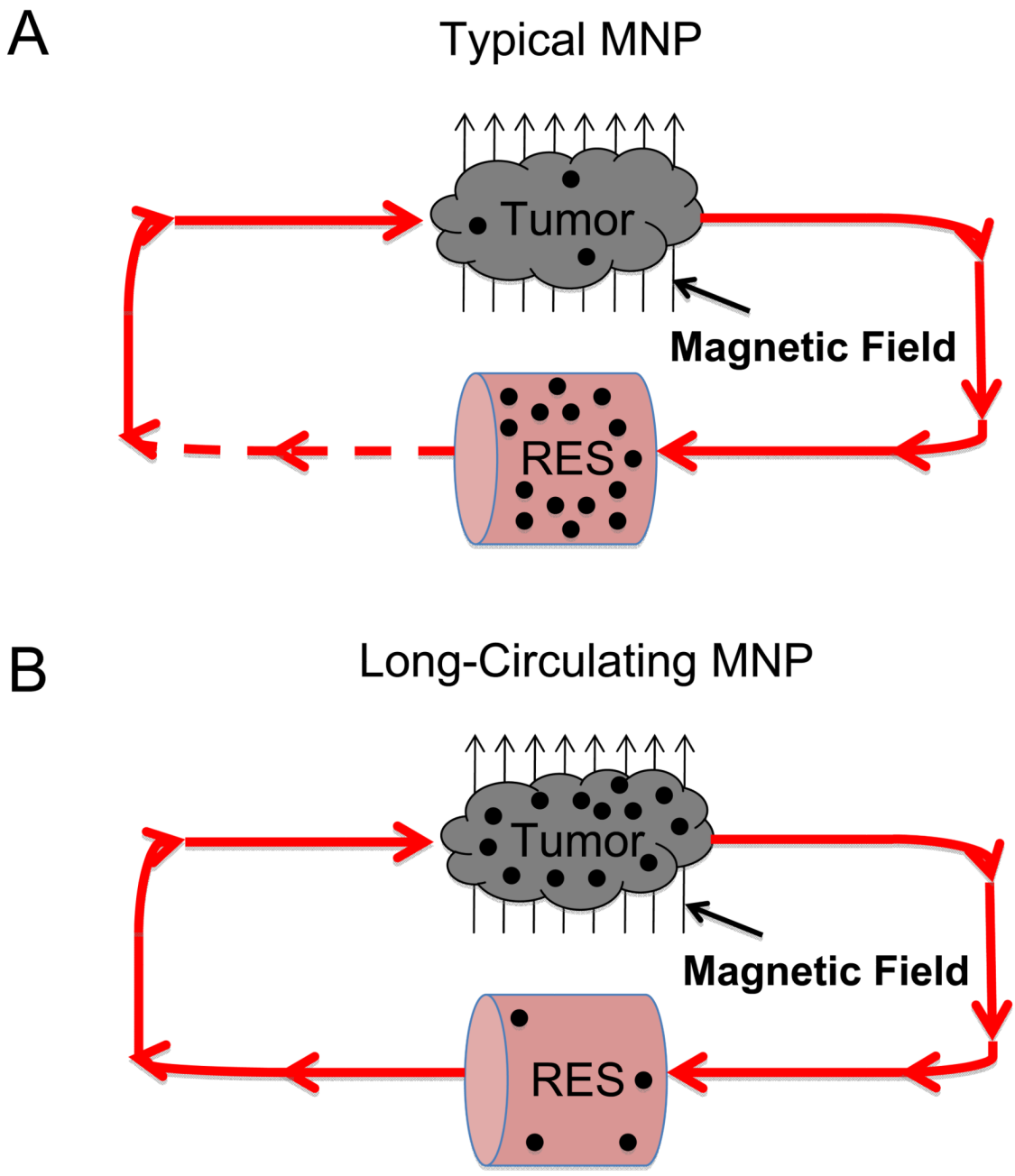

Figure 1. Conceptual schematics of enhanced magnetic brain tumor targeting hypothesis

(**A**) For a typical MNP, administered nanoparticles are quickly removed from the circulation by the RES, substantially limiting the fraction of MNPs in each pass that are returned to the tumor for additional magnetic targeting, as indicated by the dashed line (**---**). Such phenomena results in limited tumor exposure of the administered dose and, thus, limited MNP delivery. (**B**) Conversely, long-circulating MNPs, that avoid RES sequestration, would pass through tumor vasculature many times over, improving the probability of interaction with the magnetic field and, thus, achieving enhanced tumor delivery.

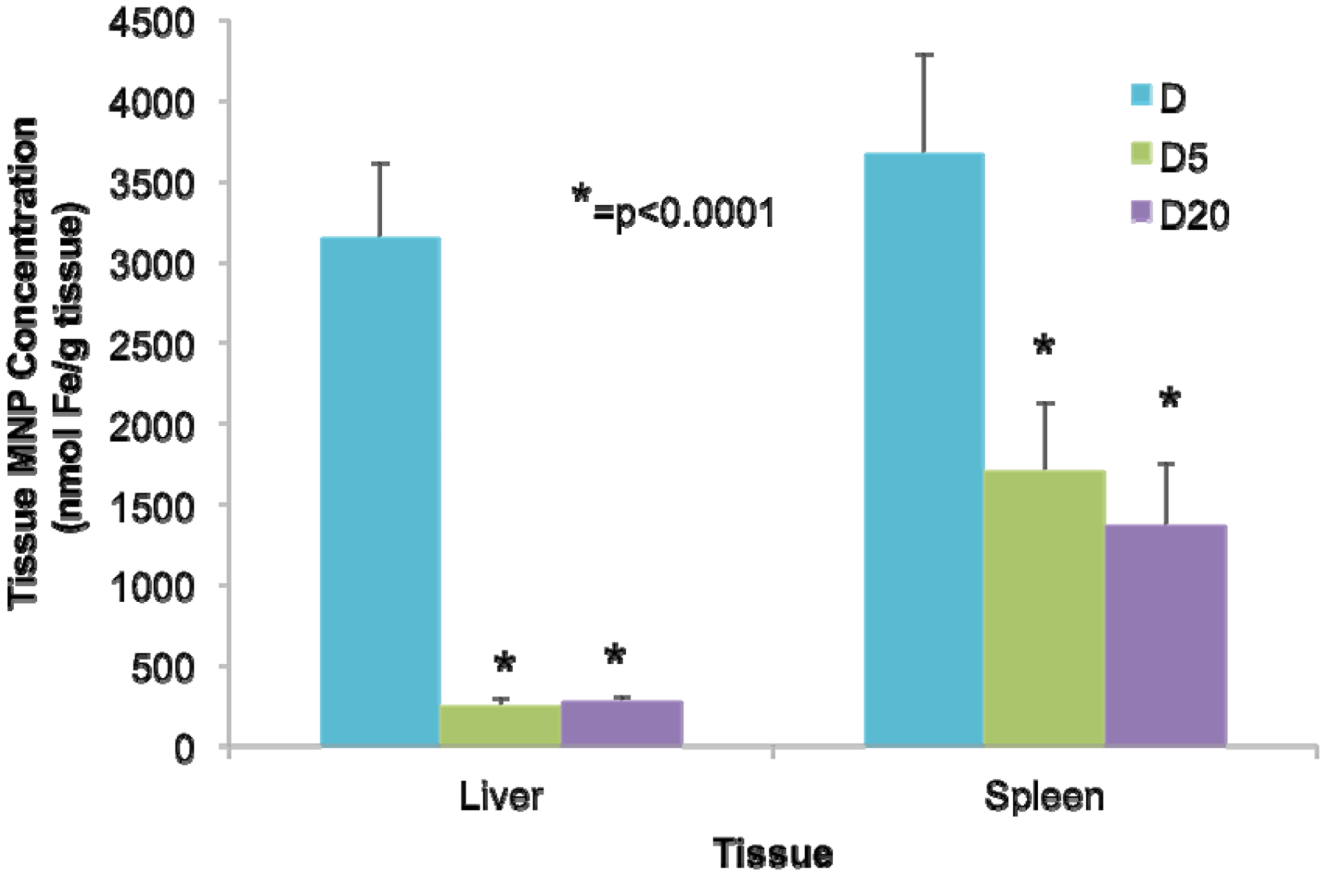

Figure 2. Comparison of D & PEG-MNP biodistribution in liver and spleen tissues (12 mg Fe/kg, 1 hr post administration, n=9)

D distributes in both the liver and spleen during plasma clearance, typical of most studied MNPs. For D5 and D20, statistically lower levels of MNPs are found in the spleen (2.2–2.6-fold reduction from D), and more dramatically in the liver (11.3–12.5-fold reduction from D). Data substantiate previously obtained pharmacokinetic results that indicate the long-circulating behavior of PEG-MNPs [16]. Moreover, the lack of proportional reductions in tissue MNP concentration between the spleen and liver suggest that the liver is distributed with PEG-MNPs to a reduced extent compared to D. Conversely, the spleen appears to possess enhanced distribution suggesting an increased role in plasma clearance of MNPs.

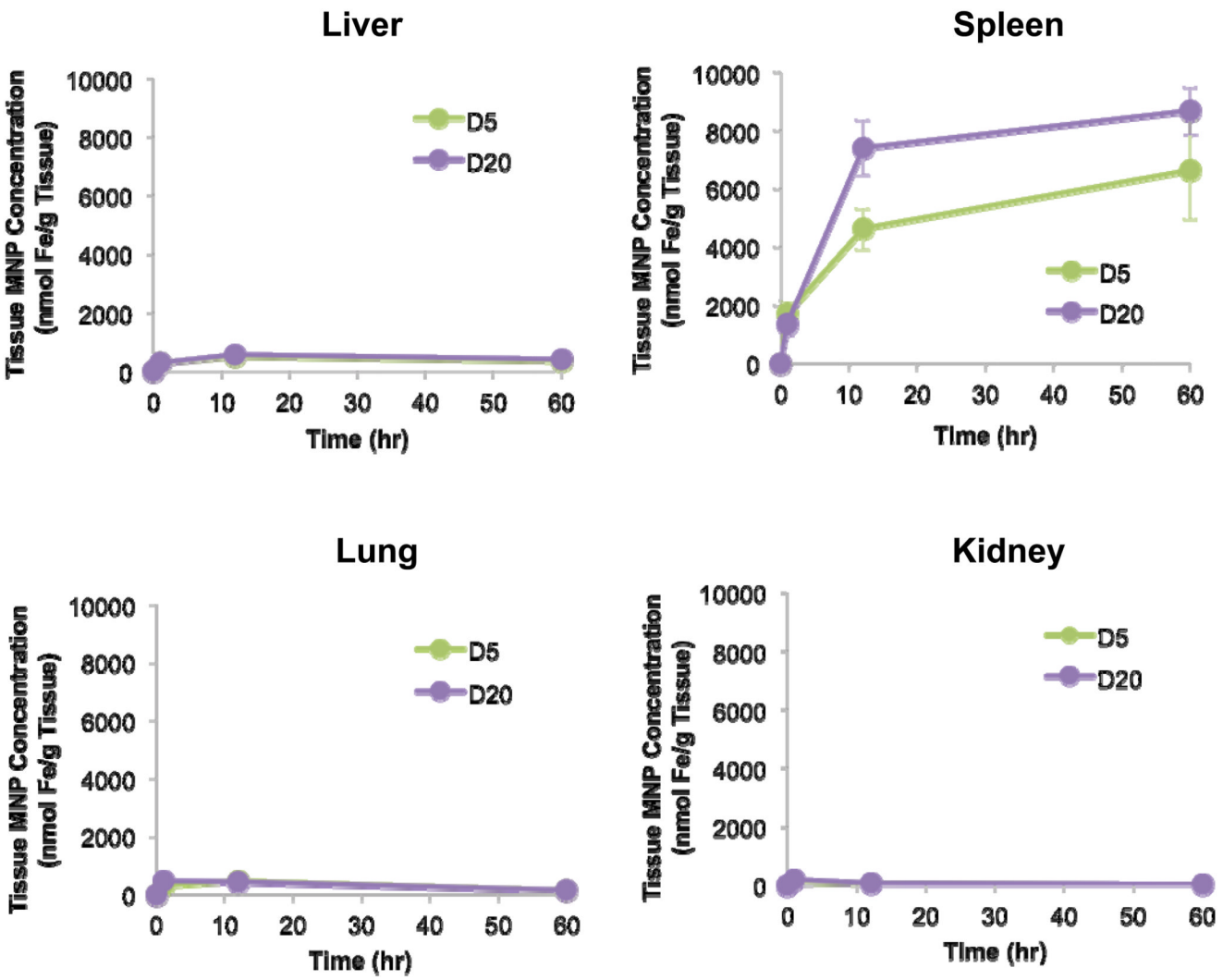

Figure 3. PEG-MNP biodistribution time course in primary organs of nanoparticle elimination (n=9)

In agreement with data in Figure 2, the spleen possesses enhanced biodistribution of PEG-MNPs throughout the time course. MNPs appear to continue to accumulate in the spleen during plasma clearance – tissue concentrations at later time points are substantially higher than that observed for D or PEG-MNPs at 1 hr. An interesting find from the data is the reduced level of MNP distribution in liver throughout the course of the run – tissue MNP concentrations remain significantly below those observed for D at 1 hour (Figure 2). Similar (to liver) levels of MNPs were measured in the lung and only minimal levels were observed in the kidney.

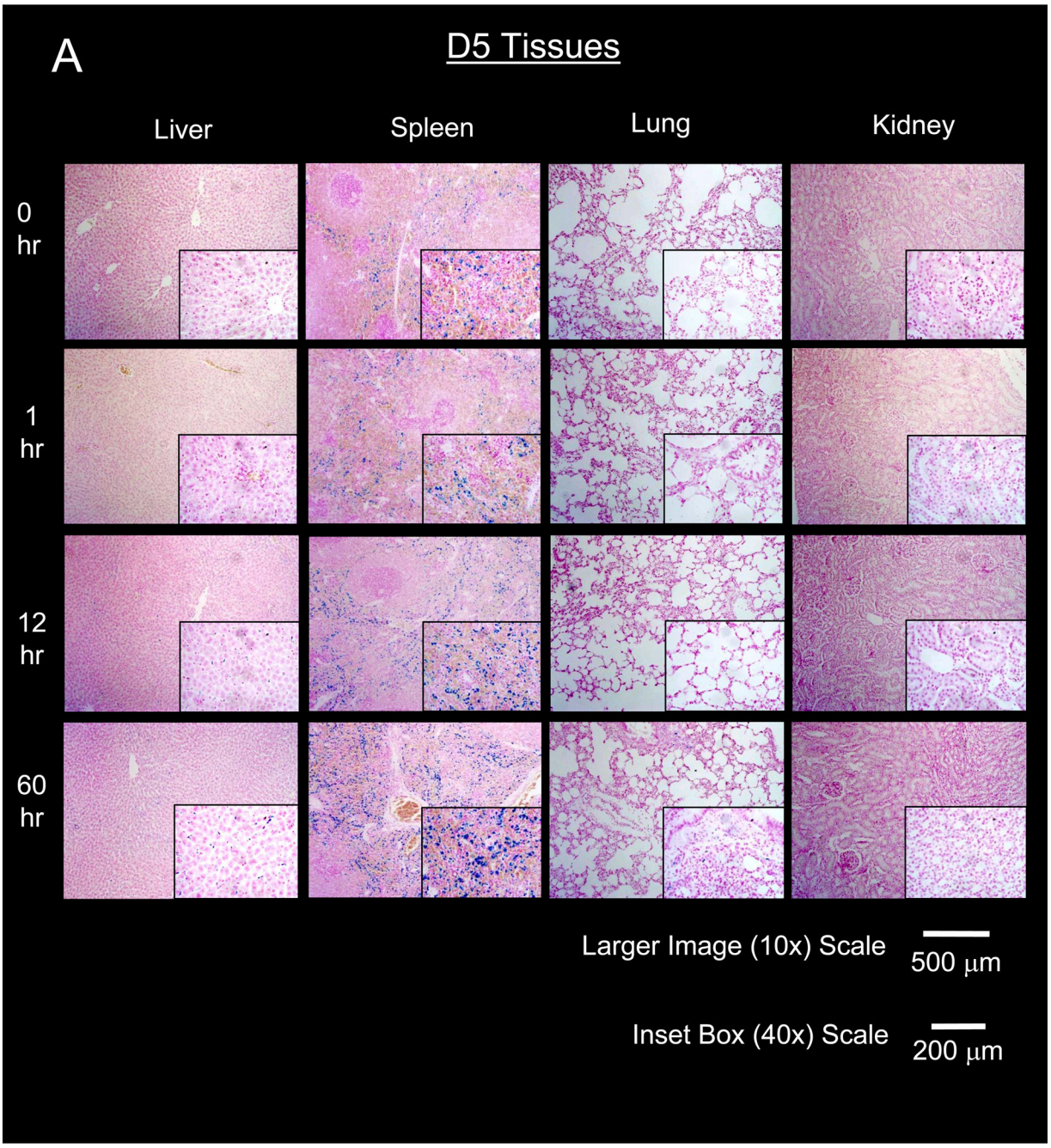

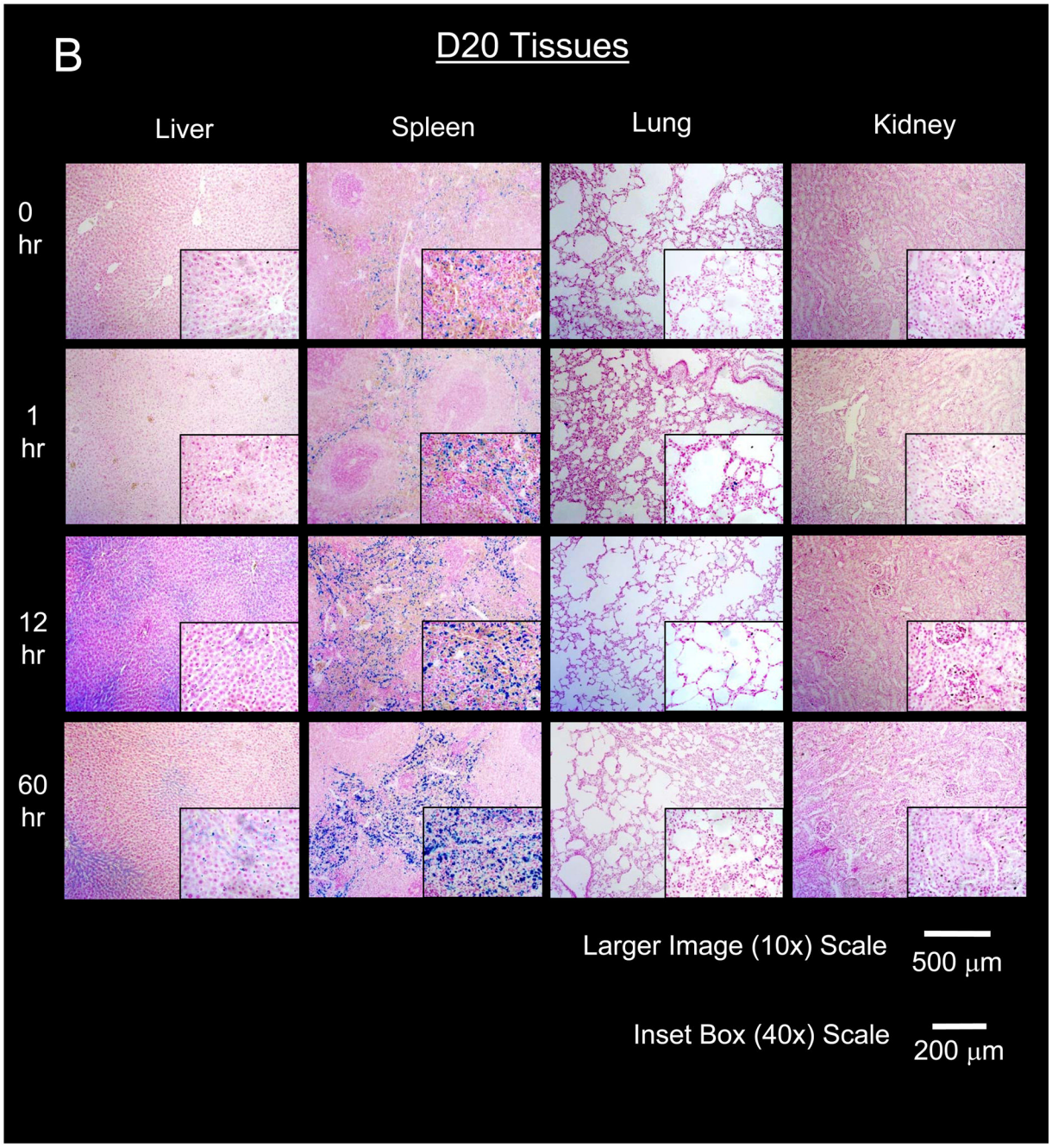

Figure 4. Histological time course of primary organs of nanoparticle elimination after administration of PEG-MNPs

Representative micrographs of elimination tissues stained to produce Prussian Blue from MNP iron and counterstained with nuclear fast red to visualize D5 (**A**) and D20 (**B**) distribution in tissues. Micrographs visually confirm tissue concentrations are high and continue to increase in the red pulp of the spleen. Increases in spleen Prussian Blue intensity over time generally agrees with quantitative data shown in Figure 3. MNP distribution is observable in the liver, at intensities less than that observed for spleen at later time points. Only minute instances of Prussian Blue can be found in lung, with no detectable distribution in the kidney for either type of nanoparticle. Lack of Prussian Blue in lung and kidney

indicates that much of the MNP content detected by ESR is limited to tissue blood that washes away during tissue preparation for histology.

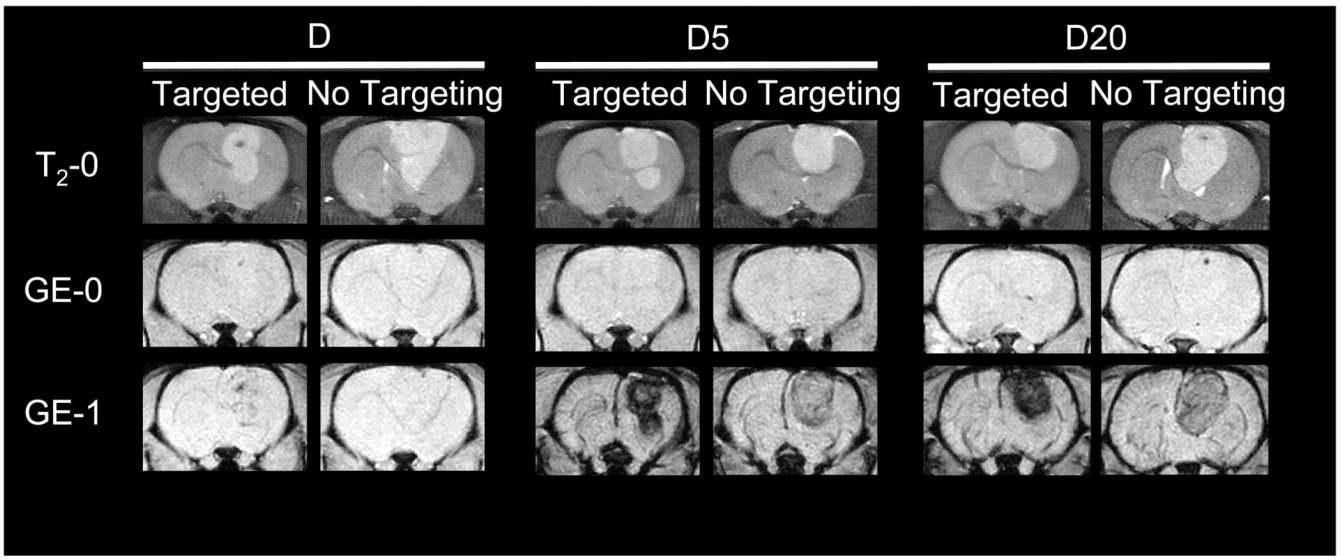

Figure 5. MRI confirmation of enhanced magnetic MNP brain tumor targeting

Representative MR images of magnetically targeted/non-targeted (t=1 hr) 9L-glioma bearing rat brain tumors after intravenous administration of D, D5, or D20 (12 mg Fe/kg). Baseline (T_2-0) T_2-weighted fast spin echo images indicate the location (hyperintense regions) of tumors in the brain. MNP presence in tissues is manifested by negative contrast (hypointensity) and is not detected on T_2*-weighted GE images at baseline (GE-0). Immediately after the conclusion of targeting at 1 hour, GE images (GE-1) show that targeting does enhance contrast in tumors over those non-targeted for each MNP tested. Tumors are dramatically darker after targeting of D5 or D20, though, when compared to parent D. Greater tumor hypointensity after targeting of PEG-MNPs indicates enhanced delivery of nanoparticles to lesions. (Images from non-targeted D first appeared in our previous work [16] and were reproduced with permission).

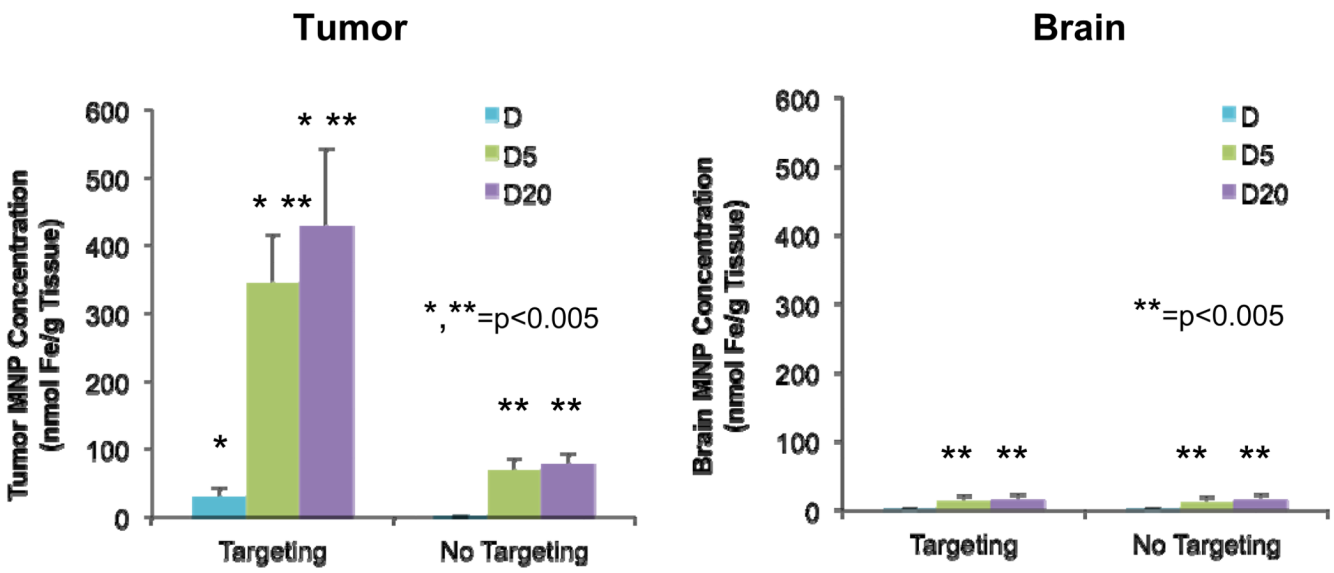

Figure 6. Quantitative *ex vivo* confirmation of enhanced magnetic brain tumor targeting of PEG-MNPs

ESR was used to evaluate MNP content in samples of tumor (n=4–5) and normal brain (n=12–15) tissues extracted from nontargeted/targeted (t=1hr) animals intravenously administered with D, D5, or D20 MNPs (12 mg Fe/kg). Enhanced tumor concentrations of targeted D5 and D20 represent 0.8% to 1.0% injected dose/g tissue compared to 0.07% injected dose/g tissue observed for targeted D. Moreover, data quantitatively confirm that the addition of magnetic targeting does not significantly increase MNP delivery to the normal brain tissue.

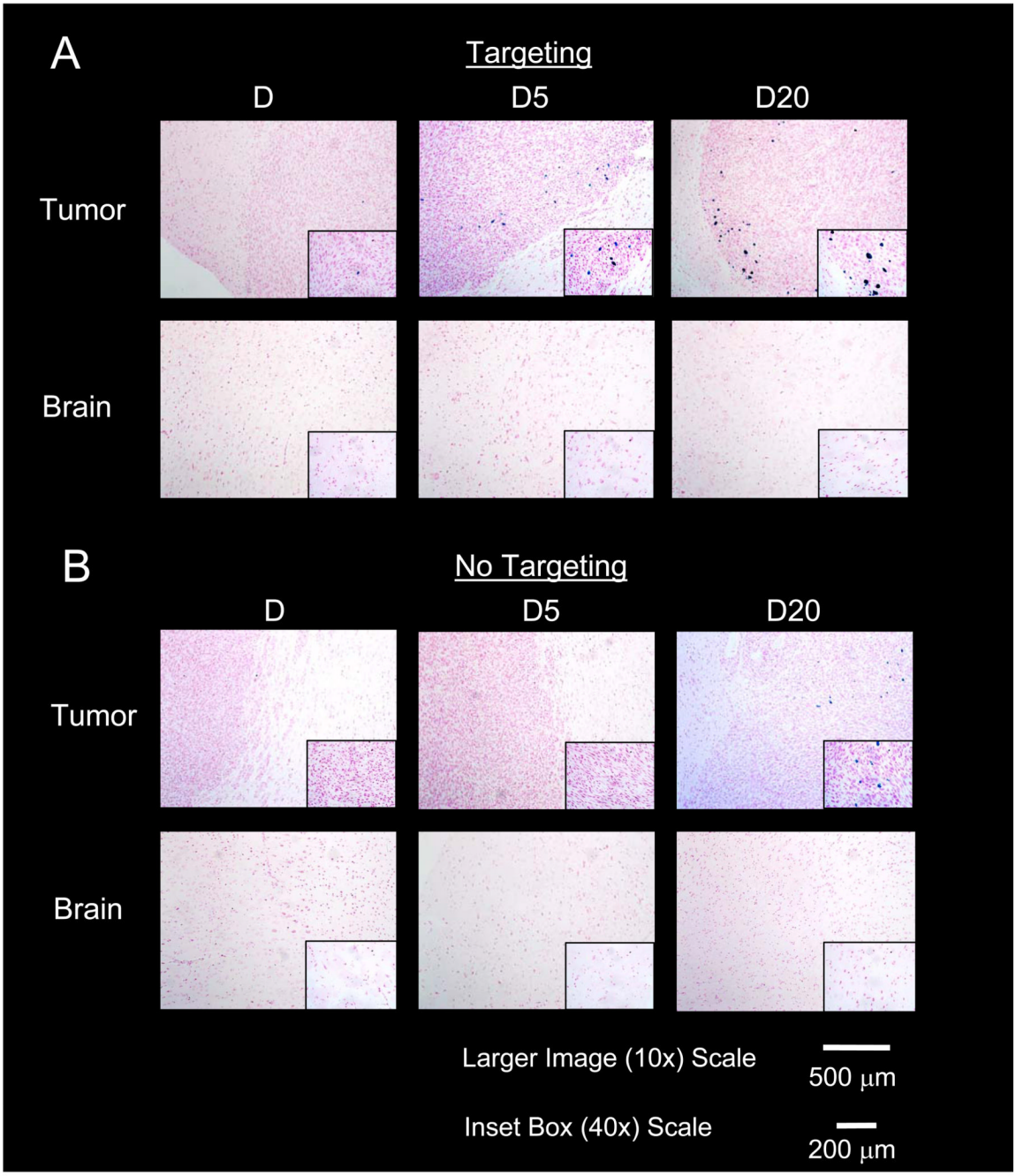

Figure 7. Histological analysis of magnetically targeted (A) and non-targeted (B) tumor and normal brain tissues

Images confirm greater retention of MNPs at the tumor site (denser cell regions) after magnetic targeting, evidenced by the Prussian Blue stained iron deposits observable in tumor tissues. Heterogeneous distribution is observed, likely due to the variably compromised BTB characteristic of a brain tumor. Conversely, little MNP accumulation is detectable in tumors not subject to magnetic targeting. Data suggest that magnetic targeting *both* captures and helps better retain MNPs at the tumor lesion, with limited passive contribution to retention. Distribution is not observed in the normal brain, with and without

targeting, even at tumor-brain boundaries. Normal brain results further confirm tumor selectivity observed in MR images in Figure 5 and ESR data in Figure 6.

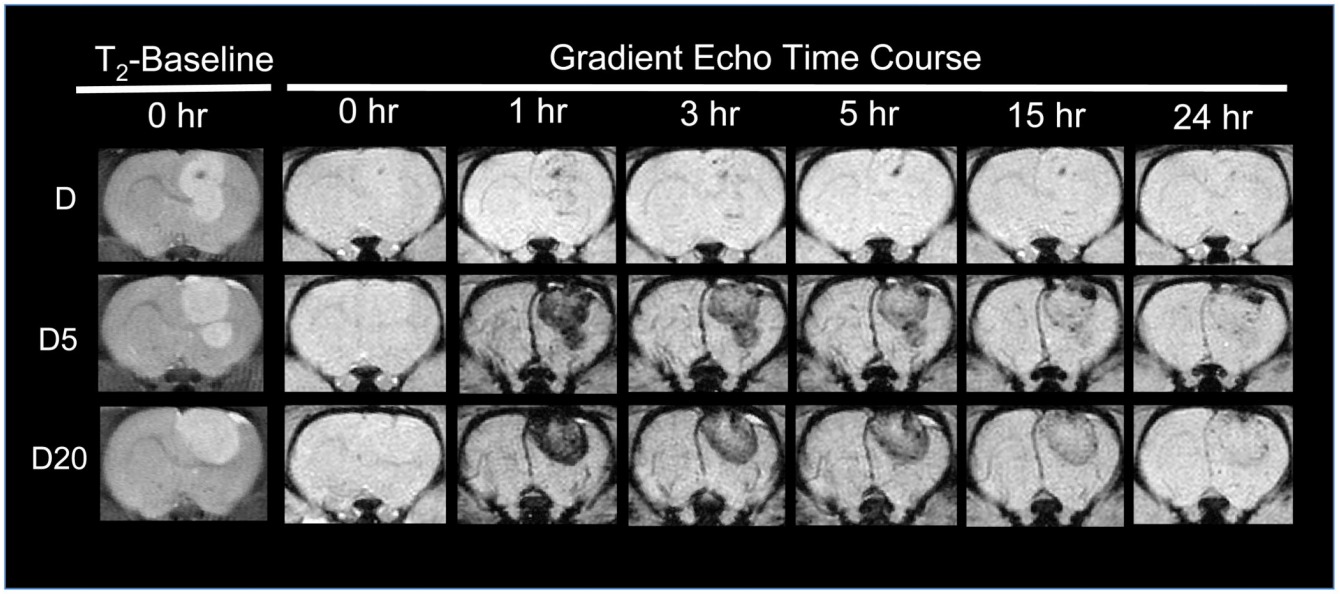

Figure 8. Visualizing post-targeting tumor clearance of D and PEG-MNPs with an MRI time course

Immediately after magnetic targeting at 1 hour, increased hypointensity can be observed in tumors, corresponding to targeted MR images shown in Figure 5. After even a short amount of time following targeting, however, the degree of hypointensity in PEG-MNP tumors is noticeably less. Data suggest that nanoparticles begin clearance from the tumor soon after cessation of the magnetic field. It is likely that the high degree of colloidal stability possessed by PEG-MNPs minimizes nanoparticle aggregation and, thus, retention in the tumor. Agglomeration-based retention likely explains the similar tumor contrast observed at 1 and 3 hours in D targeted tumors. Coupled with histology micrographs in Figure 7, data suggest the need for additional mechanisms (e.g. tumor-specific targeting ligands) to improve tumor retention of PEG-MNPs after magnetic targeting.

Table 1

Key physical and pharmacokinetic properties of D & PEG-MNPs [16]

MNP Property	D	D5	D20
Hydrodynamic diameter (nm)	104.1 ± 2.3	142.2 ± 5.6	168.5 ± 1.4
[PEG] (nmol/mg Fe)	-	4.27 ± 0.68	1.14 ± 0.25
NH_2 groups occupied by PEG (%)	-	1.45	0.39
$T_{1/2,plasma}$ (hr)	0.12	7.29	11.75
$AUC_{0-\infty,plasma}$ (μg Fe*hr/mL)	12	1182	1801

Table 2

ESR receiver gain and modulation amplitude parameters used for studies

Tissue	Receiver Gain	Modulation Amplitude (G)
Liver	5×10^4 (PEG-MNPs), 5×10^3 (D)	1
Spleen	5×10^3	1
Lung	5×10^4	1
Kidney	5×10^4	5
Brain	5×10^4	5
Tumor	5×10^4	5

Table 3

Tumor targeting advantages (TA) of PEG-MNPs with respect to various benchmarks

Benchmark	D5 Advantage	D20 Advantage
Non-Targeted Self	5.0	5.5
Targeted D	12	15
Non-Targeted D	184	229

Table 4

Tumor selectivity advantages (SA) of D & PEG-MNPs with respect to normal brain

MNP	No Magnetic Targeting	Magnetic Targeting
D	1.1	16
D5	6.0	27
D20	4.8	29